Çukurova Üniversitesi Mühendislik Fakültesi Dergisi, 39(1), ss. 175-187, Mart 2024
Cukurova University Journal of the Faculty of Engineering, 39(1), pp. 175-187, March 2024

Climbing with Robots: A Second Order Controller Design for Accurate Wheel Motion Positioning

Claudia Fernanda YAŞAR[*1] ORCID *0000-0002-8760-2359*

[1]*Yildiz Technical University, Department of Control and Automation Engineering, İstanbul, Türkiye*

Geliş tarihi: 01.05.2023 Kabul tarihi: 28.03.2024

Atıf şekli/ How to cite: YAŞAR, C.F., (2024). Climbing with Robots: A Second Order Controller Design for Accurate Wheel Motion Positioning. Cukurova University, Journal of the Faculty of Engineering, 39(1), 175-187.

Abstract

Climbing robots have become increasingly important for applications such as inspection, maintenance, and search and rescue in complex environments. This study presents studies on the design of a climbing robotic prototype that utilizes magnetic wheels for wall attachment and model-based control using algebraic second-order regulators for robust, accurate and fast positioning. The control approach uses the dynamics of the driving system with DC motors subject to high disturbance, including real physical constraints such as Coulomb friction, magnetic forces, and gravity. This controller uses pre-generated soft inputs in the form of high-order Bezier curves to reduce stall motor torques. Simulations of the robotic system's dynamic models were conducted using MATLAB, and experimental validation of the model-based control method was performed. The study validates the use of algebraic second-order controllers for monophasic DC motors to control the positioning of a climbing system subjected to high perturbations.

Keywords: Climbing robots, Motion control, Second order controllers, Robust control, Wheel positioning

Tırmanma Robotları: Hassas Tekerlek Konumlandırması için İkinci Dereceden Kontrolör Tasarımı

Öz

Tırmanma robotları, zorlu ortamlarda denetim, bakım ve arama kurtarma gibi uygulamalar için giderek önemli hale gelmiştir. Bu çalışma, duvara tutunmak için manyetik tekerleklere sahip bir tırmanma robotu sisteminin tasarımı ile dayanıklı, doğru ve hızlı konumlandırma için cebirsel ikinci dereceden model tabanlı kontrolör uygulamasını ele almaktadır. Kontrol yaklaşımı oluşturulurken, Coulomb sürtünmesi, manyetik kuvvetler ve yerçekimi gibi gerçek fiziksel kısıtlamalar da dâhil olmak üzere yüksek bozuculara maruz kalan DC motorlu sürüş sisteminin dinamik bir modeli göz önüne alınmaktadır. Bu kontrol yaklaşımında, durma motor torklarını azaltmak için yüksek dereceli Bezier eğrileri şeklinde önceden oluşturulmuş yumuşak girdiler kullanılmaktadır. Robotik sistemin dinamik modellerinin benzetim çalışmaları MATLAB ortamında gerçekleştirilmiş ve model tabanlı kontrol yönteminin deneysel uygulaması yapılmıştır. Bu

[*]Sorumlu yazar (Corresponding Author): Claudia Fernanda YAŞAR, *cfyasar@yildiz.edu.tr*

çalışma, yüksek bozucuların etkilediği bir tırmanma sisteminin konumlandırılmasını kontrol etmek için monofaze DC motorlar için cebirsel ikinci dereceden kontrolörlerin kullanımını ele almaktadır.

Anahtar Kelimeler: Tırmanma robotları, Hareket kontrolü, İkinci dereceden kontrolörler, Dayanıklı kontrol, Tekerlek konumlandırma

1. INTRODUCTION

Wall-climbing robots are mainly employed for risky and expensive tasks when executed by humans. Some of the risky jobs embrace maintenance of storage structures assessment of enormous concrete and metallic constructions such as bridges and cooling towers or dams, and examination in limited spaces. A large number of climbing robots exist in the literature, for example, robotic systems that move around on edifices, ship exteriors and many other human-made structures. The majority of climbing robots have a practical application [1]. These robots are generally used for inspection and maintenance in the ship and plane industry, petrochemical or steel surfaces of tanks, etc. [2]. Wall climbing robots with an inspection system are capable of performing non-destructive maintenance on vessels, reservoirs, scrubbers, pipelines and more. Employing sensory fusion, the climbing system can examine and measure degradation when reporting wall thickness, cracking and pitting.

The climbing robot must be enhanced with an adhesion system that sticks the robot to the wall [3,4]. This design has to consider mechanic components that adapt according to the specific surface. The mechanics of the robot and its dimensions must consider additional loads because it has to carry the necessary hardware and it is going to be affected by extra force changes coming from robot positioning (head-angle and gravity issues). The control system must be robust to high disturbances because of the friction, the magnetic forces and the gravity forces. Since the overall motor disturbance is changing in linear and nonlinear patterns, the interaction process must have strong nonlinearities [5]. Nonlinear phenomena of the Coulomb friction and the effects of gravity have a strong influence on climbing robots making them very difficult to control.

There have been multiple climbing robot designs with diverse locomotion principles. The main principles include systems that relay on arms with gripers [6], legs [7], weld lines [8], chains [9], caterpillar robots [10], wires and riels [11], etc. Arms and legs are by nature coping with the climbing strategy of insects or geckos that can ascend vertically [12]. Robots with forelegs are flexible to the surface structure and capable of bypassing obstacles. Each foot is designed separately, and equipped with adhesive components considering anticipated traction force. However, the number of degrees of freedom increases and leads to intricate mechanics and complex control designs. This also means increased weights and torques. In legged robots, the speed is reduced when compared to other ways of locomotion.

Climbing robots that make use of wheels and chains [13,14] are used on relatively smooth surfaces for fast and continuous movements. Many climbing robots use wheels or chain-driven locomotion along with locomotion and adhesion, in which the robot is equipped with suction elements [15] or uses magnetic wheels [18]. However, these systems cannot perform outsized movements or overcome objects and are exposed to slip effects.

Classical control techniques and PID controllers can be used to design effective controllers for monophasic DC motors [17]. These controllers can be tuned to achieve the desired motion or speed performance characteristics to provide stable and precise control of the motor, using tuning multiple methods. An important issue that affects motor control performance is the tuning method used to optimize control parameters.

Among the tuning methods available for motor controllers are the manual tuning method, auto-tuning, and model-based tuning. The manual method adjusts control parameters iteratively until the desired performance is achieved. This is a process that involves time and a level of expertise

in control theory. The auto-tuning method uses algorithms to automatically adjust the control parameters based on the system's response to a set of predefined input signals. It is a more efficient method than manual tuning, as it can quickly find the optimal control parameters with less human intervention. However, auto-tuning may not be suitable for systems with complex dynamics or non-linearities. The model-based tuning approach involves using mathematical models of the system to predict the optimal control parameters. Model-based tuning can provide highly accurate and robust control performance but requires detailed knowledge of the system dynamics and accurate mathematical models.

Classical control techniques can also be used to design other types of controllers, such as lead-lag compensators [19,20] and state-space controllers [21,22]. Lead-lag compensators are used to enhance stability and control time response, while state-space controllers are used to control the dynamics of the system by modelling it as a set of state equations. Fractional controllers can also be considered as a type of robust controller due to their ability to provide improved performance and stability in uncertain systems [18]. The use of fractional calculus in the controller design allows for the incorporation of non-integer order dynamics, which can account for the uncertainties and variations in the system.

The application of various motion control techniques, such as fuzzy PID control [23], adaptive sliding mode control [14], neural network-based control [25], and adaptive fuzzy along with sliding control for motion control of different types of robots and unmanned vehicles [26,27]. These techniques aim to extend the control's performance and robustness and to address the challenges posed by the uncertainties and nonlinearities of the control system. There is no need for any filtering for the measured values coming from the motor feedback.

This study presents the design and implementation of a simple climbing robotic prototype, with a magnetic wheel-based adhesion method to climb a metallic wall. The system consists of hardware, software, communication algorithms, and a sensory system based on motor encoders, which give feedback to the control system. The control approach employs a model-based control technique utilizing a reduced model of the driving system with two DC motors that are subject to high disturbances. In the work by Sira-Ramirez [28], very precise and fast Generalized Proportional Integrator (GPI) regulators are tuned using a simple algebraic methodology and are employed for tracking closely a particular reference, as well as being robust to system perturbations. These GPI controllers have been also tested for very demanding accurate trajectories for flexible beam positioning and minimal vibration [29].

This research conducts a comprehensive study of a system that includes the consideration of real physical constraints such as Coulomb friction, magnetic forces, inertia changes, and system uncertainties. In addition, this work employs simulations of the robotic system's models and control approach to guide system implementation and compare with the real-time robotic system. Furthermore, experimental validation of the dynamic models uses the platform motor's parameter estimated through experiments, and the validated dynamics are utilized for the model-based control method. Additionally, the research validates the use of algebraic GPI regulators for monophasic DC motors to control the positioning of the robotic system subjected to high perturbations. This regulator is a second-order control method to control the position of the wheels under high non-linear disturbance. This approach is an output feedback scheme that uses the measured position of the motor using an encoder. This method t does not use the disturbance model as an external compensation term. The unknown friction torque and overall disturbance are not required. There is no need for any filtering for the measured values coming from the motor encoder's feedback. This work is presented as follows: Section 2 describes the experimental climbing system. Section 3 explains the dynamic model of the system. In Section 4, the control system and its parameters are given. Section 5 presents the significant experimental results attained using the control method. The important conclusions are written in Section 6.

2. EXPERIMENTAL CLIMBING PLATFORM

This section outlines the experimental design of a climbing robotic prototype that uses two magnetic wheels. It provides information on the robot's mechanisms and features, as well as the control hardware and software used for the proposed prototype.

2.1. Mechanisms and Features

The robotic mechanisms were designed for a simple experimental platform to examine control-positioning methods for climbing with magnetic wheels. The robot was intended to climb vertical metallic walls composed of steel and was designed with two DC motors to drive the system. The authors selected magnetic adhesion for this climbing robot and noted that the additional weight results from the various extra masses the system must carry to operate, including an H bridge, a plastic base, and cables. To reduce slippage during climbing, the wheels are wrapped in elastic bands and use neodymium permanent magnets. The authors made Solidworks drawings of the robot's mechanisms and features, which are presented in Figure 1 and Figure 2. Solidworks drawings of the vertical climbing platform and its components are shown in Figure 1(a), while Figure 1(b) displays a picture of the experimental climbing prototype. Figure 2 depicts Solidworks drawings of the robotic system subjected to Coulomb, magnetic, and gravity forces.

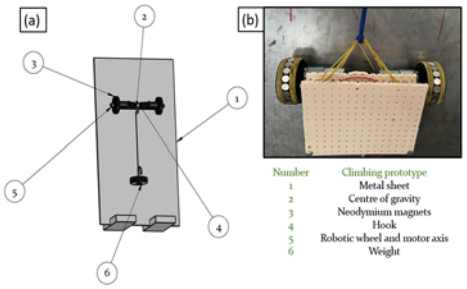

Figure 1. The magnetic wheeled climbing robot: (a) Solidworks drawings of the metallic climbing platform and the robot position, and (b) the picture of the experimental robot

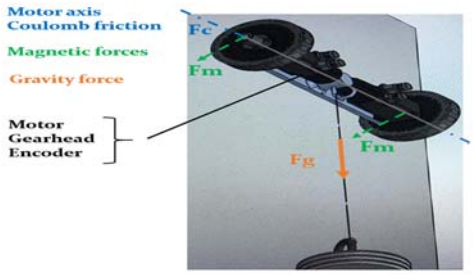

Figure 2. Solidworks drawings of the robotic system subjected to several forces.

2.2. Control Hardware and Software

The DS1104 control board, which is equipped with an MPC8240 processor and a PPC 603e core, boasts a 64-bit processor CPU, 32MB SDRAM global memory, and 8MB flash memory. The board performs data receiving and transfer operations using the input and output connections provided by the CP1104 connector panel. A PLC and CPU running under Windows are used to operate the system. The climbing robot controllers are programmed with Control Desk, which runs MATLAB/Simulink 2022(b) under Microsoft Windows 10, INTEL Core (TM) i5-7400 CPU, 3.00 GHz, and 8 GB RAM. The sampling time for real-time applications is $Ts = 1$ ms.

The control hardware includes a set of two 24 V brushed Pololu monophasic motors with a metal gearbox (18.75:1 reduction), incremental quadratic encoders with a resolution of 64 counts per revolution of the motor shaft, and an L298N Dual H-Bridge Motor driver to control the motors. The PWM signal received from an I/O Digital/Analog board is averaged to provide a proportional value of the 24 V provided by a power supply. Two incremental encoder counters are used to measure the motor's position and provide feedback to the control system.

3. DYNAMIC MODEL

This section explains a simplified model of the DC servomotor system, specifically addressing motors that are subjected to substantial disturbances. Additionally, a comprehensive depiction of the total disturbance that may affect the motor is provided.

The attainment of an accurate dynamic model, which incorporates optimal model parameters, is crucial for the implementation of a model-based control tuning approach, aimed at achieving precise and resilient control performance.

3.1. DC Motor Dynamics

A DC motor is an electromechanical component that yields an angular displacement output θ_i for a current input i_{ai}, that is, a mechanical output generated by an electrical input. In the literature, the equation related to the electrical dynamics of the motor is found to be:

$$v_{mi} = R_{ai} i_{ai} + L_{ai}\, \dot{i}_{ai} + K_{bi}\dot{\theta}_i \tag{1}$$

where *i=1,2 is* a value for each of the two motors. The applied armature voltage is denoted as V_{mi}, and the back electromotive force (emf) voltage is $V_{bi}(s) = K_{bi}\dot{\theta}_i$ where K_{bi} is the back emf constant. R_{ai} and L_{ai} are the armature resistance and inductance, respectively. The mechanical dynamics of the DC motor are described as

$$\Gamma_{mi} = K_i i_{ai} = J_i\ddot{\theta}_i + v_i\dot{\theta}_i \tag{2}$$

The variable Γ_{mi} denotes the total torque of each of the motors. Here, the motor constant is denoted as K_i. J_i stands for the rotor's inertia, while v_i denotes the viscous friction parameter. To obtain a model that relates the motor and angular position θ_i and the supplied voltage v_{mi}, the following assumptions have been made in the literature [30]: $K_{bi} = K_i$ and $L_{ai} \approx 0$. By using the Laplace transform the previous equations are yielded

$$v_{mi}(s) = R_{ai} I_{ai}(s) + L_{ai}\, \dot{\mathrm{I}}_{ai}(s) + K_i\dot{\theta}_i(s) \tag{3}$$

$$I_{ai}(\mathrm{s}) = \left(\frac{J_i\, s^2 + v_i s}{K_i}\right)\theta_i(s) \tag{4}$$

Replacing (4) in (3) and simplifying, the following transfer function is obtained:

$$\frac{\theta_i(s)}{v_{mi}(s)} = \frac{\frac{K_i}{R_{ai}\, L_{ai}}}{s\left[s + \frac{1}{J_i}\left(v_i + \frac{{K_i}^2}{R_{ai}}\right)\right]} = \frac{A_i}{s(s + B_i)} \tag{5}$$

A simplification can be made since A_i and B_i are obtained using motor parameters $A_i = \frac{K_i}{R_{ai}\, L_{ai}}$ and $B_i = \frac{1}{J_i}\left(v_i + \frac{{K_i}^2}{R_{ai}}\right)$.

A simplified transfer function $\frac{\theta_i(s)}{v_{mi}(s)}$ of a DC motor is, therefore, mathematically formulated in (5). This is the transfer function that will be used in this work and the missing part is the experimental parameter identification to find the values A_i and B_i that best represent real DC motor dynamics.

3.2. Wheel Disturbance While Climbing: Adding External Disturbance

The simplified DC model obtained in (6) is used but external disturbances affect the system while climbing, as follows:

$$\Gamma_{mi} = K_i v_{mi} = J_i\ddot{\theta}_i + v_i\dot{\theta}_i + \Gamma_{fi}(\dot{\theta}_i, v_{mi}) + \Gamma_{Ji}(v_{mi}) + \Gamma_{gi}(\theta_i) \tag{6}$$

The external disturbance torques are taken into account to give the system realistic climbing behaviour. For instance the increased rotor's inertia due to the effect of external torques, such as the magnetic forces that keep the robotic system on the metallic wall, changes in inertia due to motor positioning (such as changes in the robot's head-angle). $\Gamma_{Ji}(v_{mi})$ stands for the external torque out to changes in the rotor's inertia. $\Gamma_{gi}(\theta_i)$ denotes the effects of gravity on each of the motors. Therefore, the overall disturbance is depicted as

$$\Gamma_{di} = \Gamma_{fi}(\dot{\theta}_i, v_{mi}) + \Gamma_{Ji}(v_{mi}) + \Gamma_{gi}(\theta_i). \tag{7}$$

The overall disturbance often results in issues related to motion control, such as steady-state errors and overshooting. The Coulomb friction model is a function of the angular speed and control signal [31]. $\Gamma_{fi}(\dot{\theta}_i, v_{mi})$ can be mathematically expressed as follows:

$$\Gamma_{fi}(\dot{\theta}_i, v_{mi}) = \begin{cases} g_i(\dot{\theta}_i) & \text{if } \dot{\theta}_i \neq 0 \\ \Gamma_{si}\mathrm{sgn}(\dot{\theta}_i) & \text{if } \dot{\theta}_i = 0 \text{ \& and } |v_{mi}| \leq \frac{\Gamma_{si}}{K_i} \end{cases} \tag{8}$$

$$g_i(\dot{\theta}_i) = sgn(\dot{\theta}_i)\Gamma_{ci} + sgn(\dot{\theta}_i)(\Gamma_{si} - \Gamma_{ci})e^{-\left(\left|\frac{\dot{\theta}_i}{v_{si}}\right|\right)}$$

The proposed model incorporates several friction-related parameters, including Γ_{si}, which represents the static friction torque that gives rise to stiction phenomena when at $\dot{\theta}_i = 0$. Coulomb friction, denoted as Γ_{ci}, occurs during motion and remains constant regardless of speed. The Stribeck velocity, v_{si}, represents the sliding velocity at which only 37% of the static friction torque is active. The main DC motor parameters are given in Table 1.

3.3. DC Model and Overall Disturbance Compensation

There are two main approaches with which to deal with the compensation of the overall disturbance: first, the cancellation based on a model of the total disturbance, using its estimation and compensation; and second, the design of controllers that are robust to these effects. The first of these approaches is difficult to apply since accurate models of the total disturbance include, for example, friction with linear and non-linear patterns. To address this, high-order controllers can be employed which are controllers that compensate for the total disturbance without a prior model or estimation. In this work, the use of high-order controllers is adopted. The DC servo-motor model, its disturbance torques acting on the system, and the parameters and variables defining the simplified model are depicted in Figure 3.

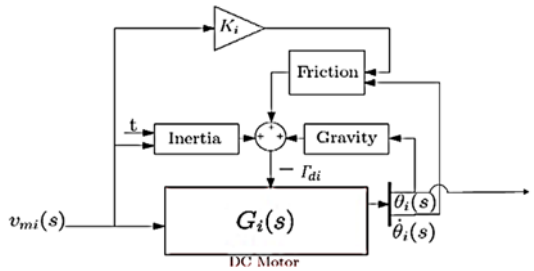

Figure 3. Block diagram: DC motor dynamics under disturbance

The system requires extra voltage to compensate for disturbances $\vartheta_i = v_{mi} + v_{fi} + v_{Ji} + v_{gi}$, where ϑ_i is the fictitious control signal of the motor required for compensation. In Figure 4, a block diagram that explains the compensation at the motor side is presented.

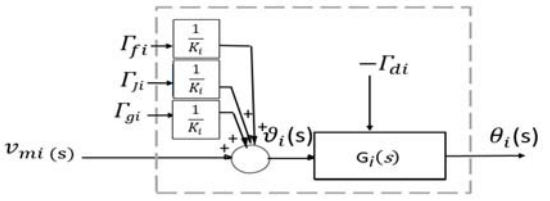

Figure 4. DC motor compensation for overall disturbance

Given that both the internal friction force and the overall disturbance (7) are adjusted, a reduced and linear differential of second order equation is derived as

$$K_i v_{mi} = J_i \ddot{\theta}_i + v_i \dot{\theta}_i \tag{9}$$

Using the Laplace transform the following equation is obtained

$$K_i v_{mi}(s) = J_i s^2 \theta_i(s) + v_i s \theta_i(s) \tag{10}$$

The transfer function $G_i(s)$ represents a simple model of the DC motor as a linear system and can be obtained from the input voltage $v_{mi}(s)$ to the resulting position θ_i(s)

$$G_i(s) = \frac{\theta_i(s)}{v_{mi}(s)} = \frac{K_i/J_i}{s\left(s + v_i/J_i\right)} = \frac{A_i}{s(s+B_i)} \tag{11}$$

The open-loop response of this system is not stable. One of the poles of the open-loop transfer function is on the left half of the complex s-plane, while the other is at the origin and behaves like an integrator. Therefore, when a step input is given its output continues to grow to infinity in the same manner that an integral of a constant grows to infinity.

3.4. DC Motor Parameter Identification: Obtaining a Reduced Experimental Dynamic Model

The robotic platform was equipped with two DC motors. MATLAB's Parameter Estimation was used to obtain motors' parameters using an experimental identification. Note: It is almost impossible to obtain a complete identification of each of the disturbances of the wheels. Therefore,

experiments are performed to obtain a close representation of the motor system. It is necessary to determine the parameters A_i and B_i of the modelled transfer function in (11), and add at least the static value of the Coulomb friction for a reduced motor model, as follows:

$$\Gamma_{mi} = K_i v_{mi} = J_i \ddot{\theta}_i + v_i \dot{\theta}_i - \Gamma_{si} \quad (12)$$

Γ_{si} represents the total torques induced by non-linear static friction in motors. In this study, these characteristics are modified to bring the reduced plant model as near to the real plant as feasible using an iterative identification process. The method is based on experiments that employ a basic closed-loop Proportional (P) controller structure, which differs from traditional open-loop approaches for parameter identification. This decision is made to allow a comparison of real and simulated systems within a closed-loop arrangement.

The first part of the experimental data is to attain the static value of the Coulomb friction. Each motor was heated up to aid the parameter identification process. Then, a PWM control signal, $v_{mi}(s)$, was applied to the motors in an open loop during the experiment, with positive and negative PWM values used for clockwise and counterclockwise motor movements, respectively. The process starts by giving very low values until the motor starts moving. The static values are PWM values right when the motor starts moving $\Gamma_{si} = \pm 0.06$ PWM.

Figure 5(a) displays the simulated closed-loop control for the reduced motor plant, as well as the controlled system response, with the experimental and simulated control responses matching to some extent. Simulated and real systems are kept comparable by employing the same proportional gains $K_p = 0.005$ and including a dead zone that simulates the static component of Coulomb friction.

The second part of the experimental identification method requires multiple experiments to achieve sufficient data to attain approximated parameters of the motors. To include clockwise and anticlockwise control responses, the experimental controller is subjected to a series of input steps that include both positive and negative values. The recorded motor input-output control data (time, reference, and output) is used as input-output for Simulink. The MATLAB parameter identification toolbox induces iterative variations in A_i and B_i to approximate the outcomes to those of the real system, as shown in Figure 5(b). The toolbox is configured to operate using a sum of square errors cost function; with the optimization method selected as non-linear least squares. The cost function iterates to find the optimal parameters that make the simulated and real model equivalent. The parameter and function tolerance is 0.001, and the maximum iteration is 100. The temporal cost function values are depicted in Figure 5(c). The resultant model is claimed to be the best-reduced model discovered by applying this procedure with parameter identification of A_i and B_i values, which are used for control purposes in this research methodology. The DC motor characteristics for both wheels are shown in Table 1.

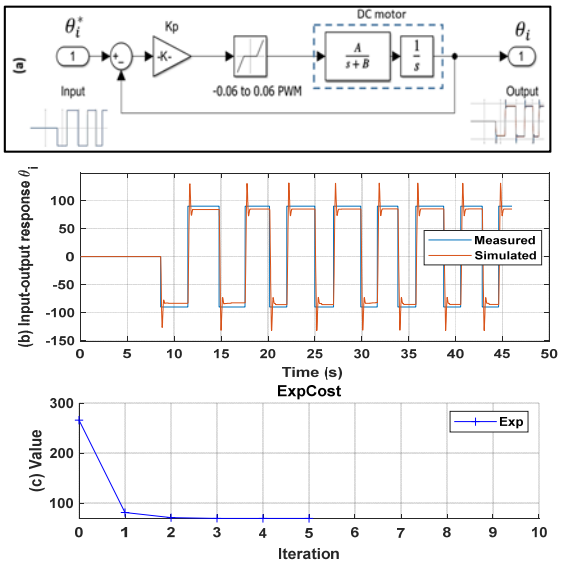

Figure 5. Experimental parameter identification, A_i and B_i, using the parameter identification toolbox of MATLAB: (a) closed-loop method based on proportional control; (b) input-output comparison for the experimental and simulated response; and (c) experimental cost function iteration by time

Table 1. DC motor model parameters

Motor left *i=1*	**Value (units)**
Parameter A_1	159 $\frac{\text{N}}{\text{V.kg.m}}$
Parameter B_1	11 $\frac{\text{N.s}}{\text{kg.m}}$
Control signal (v_{m1})	1 to -1 PWM
Static friction torque (Γ_{s1})	-0.06 ve 0.06 PWM
Motor axis inertia (J_1)	0.0018 kg. m^2
Motor constant (K_1)	0.474 N. m/V
Coulomb friction torque Γ_{c1}	0.0238 N. m
Stribeck velocity (v_{s1})	0.0105 rad/s
Motor Right *i=2*	**Value (units)**
Parameter A_2	260 $\frac{\text{N}}{\text{V.kg.m}}$
Parameter B_2	13 $\frac{\text{N.s}}{\text{kg.m}}$
Control signal (v_{m2})	1 to -1 PWM
Static friction torque (Γ_{s2})	-0.06 to 0.06 PWM
Motor axis inertia (J_2)	0.0018 kg. m^2
Motor constant (K_2)	0.474 N. m/V
Coulomb friction torque Γ_{c2}	0.0238 N. m
Stribeck velocity (v_{s2})	0.0105 rad/s

4. ALGEBRAIC SECOND ORDER CONTROLLERS

This study involves the simulation and implementation of 2-DOF algebraic PID controllers for DC monophasic motors. The objective of the design is to ensure accurate tracking of references while compensating for disturbance effects, critically damped control response with short settling time, and minimal steady-state error and overshoot. The proposed control system is required to be robust to overall disturbance through a second-order and high-gain closed-loop controller. The study utilizes various techniques to achieve these objectives, such as the use of Bezier curves for reference inputs, and comprehensive identification of motor parameters including Coulomb friction. Fast and stable responses are mandatory, therefore, the poles and allocated far from the origin and at the left side of the complex plane, while considering the sampling time ($Ts = 1$ ms) and motor saturation limits (1 to -1 PWM).

The given reduced motor dynamics is denoted by $G_i(s)$ and its associated parameter values are given in Table 1. Figure 6, illustrates the algebraic PID controller, and its tuning methodology was previously described in Castillo-Berrio [29]. The transfer function of the motor dynamics was then derived as:

$$G_i(s) = \frac{\theta_i(s)}{v_{mi}(s)} = \frac{A_i}{s(s+B_i)} = \frac{g_{n,i}(s)}{g_{di}(s)} \quad i = 1,2 \qquad (13)$$

where A_i and B_i are each of the motor parameters to describe the second-order experimental plant. $g_{n,i}(s)$ is the numerator and $g_{d,i}(s)$ is the denominator of $G_i(s)$. The controller's polynomials $n_{1,i}(s)$, $n_{2,i}(s)$ and $d_i(s)$ are defined as follows:

$$n_{1,i}(s) = a_{2,i}s^2 + a_{1,i}s + a_{0,i} \qquad (14)$$

$$n_{2,i}(s) = b_{2,i}s^2 + b_{1,i}s + b_{0,i} \qquad (15)$$

$$d_i(s) = s(s + c_{a,i}). \qquad (16)$$

Here, $a_{0,i}$, $a_{1,i}$, $a_{2,i}$, $b_{0,i}$, $b_{1,i}$, $b_{2,i}$ and $c_{a,i}$ are coefficients. The input reference for the controller is represented by $\theta_i^*(s)$, while the motor output is denoted as $\theta_i(s)$. Reference inputs are chosen based on Bezier curves due to their ability to accurately represent smooth and challenging trajectories. $M_i(s)$ is a fourth-order transfer function and can be expressed as:

$$M_i(s) = \frac{\theta_i(s)}{\theta_i^*(s)} = \frac{G_i(s)n_{1,i}(s)}{d_i(s) + G_i(s)(n_{1,i}(s) + n_{2,i}(s))} \qquad (17)$$

This is a closed-loop transfer function whose characteristic equations have four poles each of them placed in p_i. The control settings are then

$$d_i(s)g_{d,i}(s)+g_{n,i}(s)(n_{1,i}(s)+n_{2,i}(s))=(s-p_i)^4 \qquad (18)$$

$d_i(s)$ includes a root at the origin. Equation (18) offers four conditions to tune seven parameters. Multiple real poles all placed on the left side of the complex plane are selected to provide critically damped responses. Replacing all the parameters in the closed-loop transfer function of the controlled system the following transfer function is obtained

$$M_i(s) = \frac{\theta_i(s)}{\theta_i^*(s)} = \frac{A_i\left(a_{2,i}s^2 + a_{1,i}s + a_{0,i}\right)}{s^4 + \left(c_{a,i} + B_i\right)s^3 + \left(c_{a,i}B_i + a_{2,i}A_i + b_{2,i}A_i\right)s^2 + \left(a_{1,i}A_i + b_{1,i}A_i\right)s + \left(a_{0,i}A_i + b_{0,i}A_i\right)} \quad (19)$$

The control response must achieve zero static error for both step inputs and step disturbance. Then, using the final value theorem makes it easy to demonstrate the condition $b_{0,i} = 0$. Additional conditions are required to be defined, for instance, by selecting $n_{1,i}(s)$ to make the gain of $M_i(s)$ equal to one, and two zeroes of the transfer function $M_i(s)$ cancel two poles. The zeroes can be written as

$$s^2 + \frac{a_{1,i}}{a_{2,i}}s + \frac{a_{0,i}}{a_{2,i}} = (s^2 - 2p_i s + {p_i}^2) = (s - p_i)^2 \quad (20)$$

By matching the coefficients of both sides of the equation the following conditions must be met $\frac{a_{1,i}}{a_{2,i}} = -2p_i$ and $\frac{a_{0,i}}{a_{2,i}} = {p_i}^2$. Therefore, seven equations to calculate seven parameters are yielded. Then, arranging $a_{1,i}$ and $a_{0,i}$ in terms of $a_{2,i}$ and replacing the conditions in the denominator of the closed loop transfer function characteristic equation is given in terms of the closed loop poles p_i. The controller parameter equations are given in Table 2.

Table 2. Equations to calculate the algebraic second-order controller parameters

$a_{0,i}$	$\boldsymbol{a_{1,i}}$	$\boldsymbol{a_{2,i}}$	$\boldsymbol{c_{a,i}}$
$\frac{\boldsymbol{p_i}^4}{\boldsymbol{A_i}}$	$\frac{-2{p_i}^3}{A_i}$	$\frac{{p_i}^2}{A_i}$	$-4p_i - B_i$
$\boldsymbol{b_{0,i}}$	$b_{1,i}$	$b_{2,i}$	
0	$\frac{-2{p_i}^3}{A_i}$	$\frac{-5{p_i}^2}{A_i} + \frac{(4p_i + B_i)B_i}{A_i}$	

After the zero pole cancellation, the new closed-loop transfer functions denominator is of second order and can be expressed as:

$$M_i(s) = \frac{\theta_i(s)}{\theta_i^*(s)} = \frac{1}{(1 + \alpha_i s)^2} \quad (21)$$

In this work, each motor is individually controlled and the closed-loop dynamics may be written as:

$$\theta_i^*(s) = \theta_i(s) + 2\dot{\alpha}_i\dot{\theta}_i(s) + \alpha_i^2\ddot{\theta}_i(s) \quad (22)$$

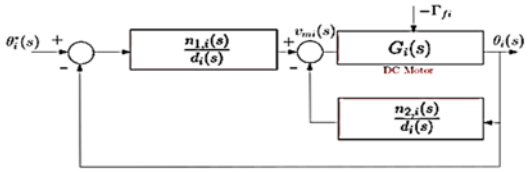

Figure 6. Algebraic second-order controller.

This Routh-Hurwitz matrix specifies mathematical conditions for determining whether a particular linear system is asymptotically stable based on the signs of the coefficients of its characteristic polynomial. The system is stable if all of the signs in the first column are positive. Sign alterations indicate the presence of unstable poles. After meeting, the constraints mentioned to derive the algebraic second-order controller parameters in Section 4, and using (18), replacing the motor parameters A_i and B_i, and noting that the closed loop poles p_i must be negative, the following polynomial is obtained:

$$s^4 + \left(c_{a,i} + 11\right)s^3 + \left(11\,c_{a,i} + 159\,a_{2,i} + 159b_{2,i}\right)s^2 + \left(159b_{1,i} - 318\,a_{2,i}p_i\right)s + 159a_{2,i}{p_i}^2 = P(s) \quad (23)$$

According to the stability criterion used on the Routh Hurwitz matrix's first column obtained

$$a_4 = 1 > 0$$
$$a_3 = (c_{a,i} + 11) > 0$$
$$b_1 = \frac{\left(159b_{1,i} - 318\,a_{2,i}p_i\right)\left(c_{a,i} + 11\right) - \left(11\,c_{a,i} + 159\,a_{2,i} + 159b_{2,i}\right)}{\left(c_{a,i} + 11\right)} > 0 \quad (24)$$
$$c_1 = \left(159b_{1,i} - 318\,a_{2,i}p_i\right) > 0$$

* If $c_{a,i} > -11$, then the system is stable.
* Let's denote $N = (159b_{1,i} - 318\,a_{2,i}p_i)(c_{a,i} + 11) - (11\,c_{a,i} + 159\,a_{2,i} + 159b_{2,i})$; the term $(159b_{1,i} - 318\,a_{2,i}p_i)$ has the same sign as $(11\,c_{a,i} + 159\,a_{2,i} + 159b_{2,i})$ because p_i is always negative. The term $-(11\,c_{a,i} + 159\,a_{2,i} + 159b_{2,i})$ is always negative. Then, N has the same sign as $(c_{a,i} + 11)$ and contributes to stability.
* The term $(159b_{1,i} - 318\,a_{2,i}p_i)$ must have the same sign as p_i. If $p_i < 0$, then the term $(159b_{1,i} - 318\,a_{2,i}p_i)$ is positive. Therefore, $(159b_{1,i} - 318\,a_{2,i}p_i)$ is stable.

5. CONTROL SETUP AND RESULTS

The algebraic second-order control's poles and parameters and four multiple poles placed at p_i for each of the poles and both controllers θ_1 and θ_2, left and right motor, respectively. Three different experimental cases were performed to test the robotic prototype's control system while climbing a vertical wall made of steel. Table 3 provides the calculated algebraic second-order control parameters.

Table 3. Algebraic second-order control parameters.

i	Poles p_i	$a_{0,i}$	$a_{1,i}$	$a_{2,i}$	$b_{0,i}$	$b_{1,i}$	$b_{2,i}$	$c_{a,i}$
θ_1	-50	24038	962	10	0	962	38.7	187
θ_2	-50	39308	1572	16	0	1572	65.5	189

5.1. Experimental Case 1: Bezier Curves and Step Input as Control References

Bezier curves are high-order curves that provide smooth profiles that can be utilized as inputs in control systems. In an initial experiment, a fast Bezier curve is employed, with the reference point moving from 0 to pi/3 radians in 0.3 seconds. This curve serves as the reference input for an algebraic second-order controller and is compared to a simple step input of pi/3 radians. The performance of the algebraic second-order controller in response to both inputs is shown in Figure 7. Specifically, Figure 7(a) displays the inputs at two time intervals, along with the corresponding controller output responses. The motor controller performs exceptionally well in following the challenging trajectory and tracking the shape of the Bezier curve. In Figure 7(b), the required control signal to execute the control manoeuvre is depicted. When compared to the step input, the required effort for the pre-designed Bezier curve is substantially lower, with the controller becoming saturated in the case of the step input. Figure 7(c) shows the control errors, with the error being significantly lower when using a pre-designed curve, and considerably higher when using a classical step input. To meet the high-performance requirements for wheel climbing, pre-designed Bezier curves are an essential component of our control strategy.

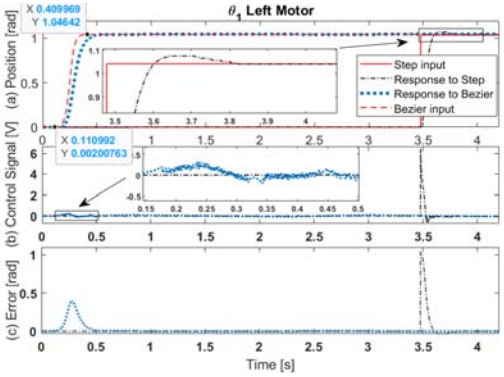

Figure 7. Bezier curves and step inputs for motion control performance

5.2. Experimental Case 2: Simulation and Real-Time Control Performance

The dynamic models, DC motor models, disturbance models, and designed controllers have been simulated, and the simulation results suggest that algebraic second-order controllers can be used for climbing robotics. The simulation results, which include the performance of both θ_1 and θ_2 motors controlled separately, demonstrate that the Bezier inputs, which range from 0 to pi/3 radians in 0.8 seconds, can be tracked successfully. Figure 8(a) illustrates the system's references and control response for the requested motion manoeuvre, while Figure 8(b) displays the control signal requested for the manoeuvre, which always remained lower than the maximum control limits (PWM +1,-1). In Figure 8(c), the error maximum values were lower than 0.1 radians in both transient responses. These figures demonstrate that the

control models have good tracking performance and that the real-time control implementation is effective. The simulation results indicate that the dynamic and control designs are close approximations of the real-time results, and these simulations can be used to represent and actuate the robotic system successfully.

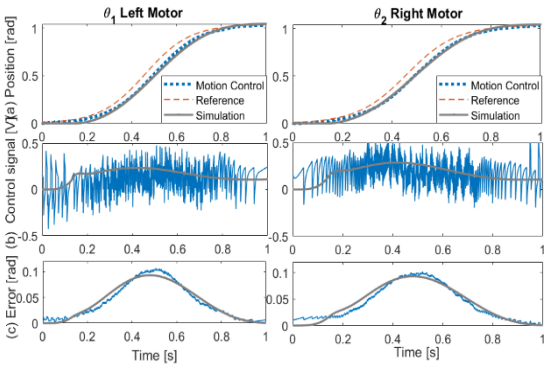

Figure 8. θ_1 and θ_2 simulation and real-time control performance: (a) Algebraic second-order controller for motion control, (b) Control signal, and (c) controller's error

5.3. Experimental Case 3: Evaluating the Transient and Steady State Control Response

The climbing robotic prototype was tested by performing a long trajectory, during which it climbed three steps up and three steps down, returning to its initial position. Each independent manoeuvre ranged from 0 to pi/3 radians in 0.8 seconds. Figure 8 illustrates the remarkable control tracking of both controllers for motors, θ_1 and θ_2, for the long trajectory, allowing for observation of both the transient and steady-state response. Figure 9(a) displays the input-output control results, while Figure 9(b) shows the required control effort. The control signals do not saturate, except for some isolated milliseconds that have minimal effect on control performance. For the majority of the experimental time, the system does not undergo abrupt values that would saturate the motor. The control error only reaches 0.1 radians while surpassing the transients, and is minimal for the steady-state response, as depicted in Figure 9(c).

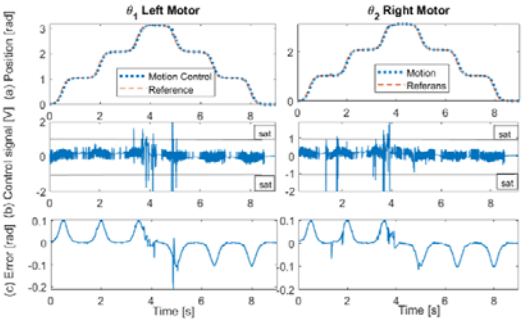

Figure 9. θ_1 and θ_2 real-time control performance while performing a log trajectory: (a) Control positioning response, (b) the required control signal, and (c) the control error

6. CONCLUSION

This study presents a two-wheeled climbing robot design that utilizes magnetic wheels for wall attachment and algebraic second-order regulators as model-based controllers for accurate motion positioning. The developed system includes hardware, software, communication algorithms, and a sensory system based on motor encoders. The control approach uses a model-based control approach that uses a DC motor driving dynamics and considers real physical constraints such as Coulomb friction, magnetic forces, and gravity forces.

Simulation and experimental validation of the control system while climbing have been performed to support the accuracy of the control approach. The controller employs pre-generated soft inputs in the form of high-order Bezier curves to reduce large stall motor torques when driving the DC motors. The results demonstrate that algebraic second-order regulators can be successfully used for monophasic DC motors to control the positioning of the robotic system subjected to high perturbations. Experimental results show that the control signals remain within the maximum control limits and that the control error is minimal, reaching only 0.1 radians while surpassing the transients. Overall, this research contributes to the field of climbing robotics and offers insights into the development of high-

performance model-based controllers for motion positioning.

Future work will involve the implementation of intelligent control methods to enhance the robustness and accuracy of the controllers, and the assessment of the proposed methods under varying loading conditions in a climbing scenario. Additionally, the system can be extended to develop a fully instrumented and robust four-wheeled robotic prototype.

7. ACKNOWLEDGEMENTS

This work has been supported by the Scientific and Technological Research Council of Türkiye (TÜBITAK) under Project 121E450 (3501 - KARIYER GELISTIRME PROGRAMI).

8. REFERENCES

1. Schmidt, D., Berns, K., 2013. Climbing Robots for Maintenance and Inspections of Vertical Structures. A Survey of Design Aspects and Technologies. Robotics and Autonomous Systems, 61(12), 1288-1305.

2. Chang, Y., Chen, X., 2015. Design of a Scalable Wall Climbing Robot for Inter-Plane Traversing, Robotic Welding, Intelligence and Automation. Advances in Intelligent Systems and Computing, 363, 309-313.

3. Shen, W., Gu, J., Shen, Y., 2005. Permanent Magnetic System Design for the Wall-Climbing Robot. Proceedings of the IEEE International Conference on Robotics and Automation, 4, 2078-2083.

4. Yoshida, Y., Ma, S., 2010. Design of a Wall-Climbing Robot with Passive Suction Cups. Proceedings of the IEEE International Conference on Robotics and Biomimetics, 1513-1518.

5. Zheng-Yi, X., Zhang, K., Xiao-Peng, Z. Hao, S., 2015. Design and Optimization of Magnetic Wheel for Wall Climbing Robot. Springer International Publishing.

6. Peidró, A., Tavakoli, M., Marín, J.M., Reinoso, Ó., 2019. Design of Compact Switchable Magnetic Grippers for the HyReCRo Structure Climbing Robot, Mechatronics, 59, 199-212.

7. Bi, Z.Q., Guan, Y.S., Chen, S.Z., 2012. A Miniature Biped Wall-Climbing Robot for Inspection of Magnetic Metal Surfaces. Proceedings of the IEEE International Conference on Robotics and Biomimetics, 324-329.

8. Gallegos, G., Sattar, T., Corsar, M., James, R., Seghier, D., 2018. Towards Safe Inspection of Long Weld Lines on Ship Hulls Using an Autonomous Robot. 21st International Conference on Climbing and Walking Robots (CLAWAR 2018), Panama, 10-12 Sep.

9. Huang, H., Li, D., Xue, Z., Chen, X., Liu, S., Leng, J., Wei, Y., 2017. Design and Performance Analysis of a Tracked Wall-Climbing Robot for Ship Inspection in Shipbuilding. Ocean Engineering, 131, 224-230.

10. Wang, W., Wang, Y., Wang, K., Zhang, H., Zhang, J., 2008. Analysis of the Kinematics of Module Climbing Caterpillar Robots. IEEE/ASME International Conference on Advanced Intelligent Mechatronics (AIM 2008), 84-89.

11. Kitai, S., Tsuru, K., Hirose, S., 2005. The Proposal of Swarm Type Wall Climbing Robot System Anchor Climber Design and Examination of the Adhering Mobile Unit. IEEE/RSJ International Conference on Intelligent Robots and Systems, 475-480.

12. Yu, Z., W., Shi, Y., Xie, J.X., Yang, S.X., Dai, Z.D., 2018. Design and Analysis of a Bionic Adhesive Foot for a Gecko Robot Climbing the Ceiling. International Journal of Robotics and Automation, 33, 445-454.

13. Zhang, Y., Dai, Z., Xu, Y., Qian, R., 2019. Design and Adsorption Force Optimization Analysis of TOFD-Based Weld Inspection Robot. Journal of Physics: Conference Series, 1303, The Second International Conference on Mechanical, Electric and Industrial Engineering 25-27 May 2019, Hangzhou, China.

14. Milella, A., Maglietta, R., Caccia, M., Bruzzone, G., 2017. Robotic Inspection of Ship Hull Surfaces Using a Magnetic Crawler and a Monocular Camera. Sens. Rev., 37, 425-435.

15. Yoshida, Y., Ma, S., 2010. Design of a Wall-climbing Robot with Passive Suction Cups.

IEEE International Conference on Robotics and Biomimetics, Tianjin, 1513-1518.
16. Fischer, W., Caprari, G., Siegwart, R., Moser, R., 2012. Compact Climbing Robot Rolling on Flexible Magnetic Rollers for Generator Inspection with the Rotor Still Installed. Industrial Robot: An International Journal, 39, 236-241.
17. Chen, Y., Zhang, J., Liu, H., Chen, Z., 2022. A New PID Tuning Method for DC Motors Based on Fractional Order Integral Criterion. ISA Transactions, 123, 211-219.
18. Kim, J., Kim, D., 2021. Development of a High-Precision Position Control System Using a PID Controller for a Monophasic DC Motor. Applied Sciences, 11(10), 4654.
19. Li, X., Li, Y., Li, Z., Zhang, L., 2022. Adaptive Fuzzy Sliding Mode Control for Position Tracking of DC Motor with Lead-Lag Compensator, International Journal of Control. Automation and Systems, 20(1), 382-392.
20. Kim, J., Kim, D., 2022. A Robust Position Control System Using a Lead-Lag Compensator for a Monophasic DC Motor. IEEE Transactions on Industrial Electronics, 69(1), 767-777.
21. Chen, G., Yu, Z., Du, R., 2022. State Feedback Control of a DC Motor Based on Sliding Mode Observer. Journal of Control and Decision, 7(2), 220-227.
22. Han, X., Wang, F., 2021. Design and Implementation of State Space Control for DC Motor Based on System Identification. Journal of Control and Decision, 6(3), 307-314.
23. Yu, Z., Chen, X., Zhang, Y., Chen, W., 2021. Design and Simulation of a Motion Control System for a Quadrotor Based on Fuzzy PID Control. Aerospace Science and Technology, 120, 106082.
24. Huang, Y., He, S., Zhang, W., 2021. Adaptive Sliding Mode Control for the Motion Control of Robot Manipulators with Parameter Uncertainties. International Journal of Control, Automation and Systems, 19(2), 652-661.
25. Karakas, B., Arslan, E., Sekercioglu, A., 2021. Neural Network-based Robust Motion Control for a Robotic System with a 3-DOF Planar Parallel Manipulator. Robotics and Computer-Integrated Manufacturing, 69, 101992.
26. Zhang, H., Yu, H., 2022. An Adaptive Fuzzy Control Approach for Motion Control of an Underwater Robot with an Unknown Payload. Ocean Engineering, 252, 108851.
27. Li, Y., Li, J., Dong, W., Li, C., 2022. Robust Motion Control for a Flexible Joint Robot Using Adaptive Fuzzy Sliding Mode Control. Robotics and Computer-Integrated Manufacturing, 73, 101974.
28. Sira-Ramirez, H., Agrawal, S.K., 2004. Differential Flat Systems, 17. CRC Press.
29. Castillo-Berrio, C., Feliu, V., 2015. Vibration-Free Position Control for a Two-Degrees-of-Freedom Flexible-Beam Sensor. Mechatronics, 27.
30. Nise, N.S., 2015. Control Systems Engineering, 7_{th} ed. California, John Wiley Sons.
31. Olsson, H., Åström, K.J., Canudas de Wit, C., Gafvert, M., Lischinsky, P., 1998. Friction Models and Friction Compensation. European Journal of Control, 4(3), 176-195.